Reduced reaction mechanisms for Sustainable Aviation Fuel (SAF): isoparaffinic alcohol-to-jet Synthetic Paraffinic Kerosene (AtJ-SPK) and its blends with Jet A

Jiangkuan Xing,* Zhenhua An, Yanqi Zhang, and Ryoichi Kurose

Department of Mechanical Engineering and Science, Kyoto University, Kyoto daigaku-Katsura, Nishikyo-ku, Kyoto 615-8540, Japan

E-mail: xing.jiangkuan.6h@kyoto-u.ac.jp

Abstract

Alcohol-to-jet Synthetic Paraffinic Kerosene (AtJ-SPK), an approved sustainable aviation fuel (SAF) by blending with conventional Jet A fuel, has recently been experimentally and studied, and detailed mechanisms have been developed to describe its combustion behavior. The present study aims to develop reduced mechanisms of AtJ-SPK and its blends with Jet A for high-fidelity and computationally-affordable Computational Fluid Dynamics. Specifically, two reduced mechanisms were developed for pure AtJ-SPK and its blends with Jet A from the LLNL-AtJ-SPK (Richter et al., Combust. Flame 240 (2022) 111994) and POLIMI detailed mechanisms (Ranzi et al., Prog. Energy Combust. Sci. 38(4) (2012) 468-501), respectively, using a combined reduction method. The reduced mechanisms can achieve 80%/92.4% and 92%/90% reductions of the species/reaction numbers, respectively, compared with those of the master detailed mechanisms. The developed reduced mechanisms were further validated under various conditions, by comparing the predicted ignition delay times, laminar flame speeds,

and temporal/spatial profiles with those predicted using the master detailed mechanisms as well as experimental data. Finally, the computational cost comparison in the two-dimensional direct numerical simulation demonstrated that the developed reduced mechanisms can impressively accelerate the calculation speed by more than 5000 and 529 times, respectively.

1 Introduction

The environmental issue of global warming caused by greenhouse gas emissions has become increasingly prominent in the recent decades. Carbon dioxide (CO_2), as one of the primary greenhouse gas, is mainly emitted from human production and life.[1] The use of sustainable aviation fuel (SAF) is regarded as one of the promising and efficient methods for reducing carbon emission from the aviation industry.[2–4] According to the review of technical pathways for SAF application summarized by U.S. Department of Energy,[5] seven SAFs, from Annex A1 to A7, have been qualified with the ASTM D4054[6] tests and their pathways were included under ASTM D7566[7] through blending with conventional jet fuels under certain maximum ratios[2,4]. Alcohol-to-Jet Synthetic Paraffinic Kerosene (AtJ-SPK), Annex A5, is one of the approved SAFs, which was developed by Gevo company and approved to co-fire with conventional Jet A/Jet A-1 at a maximum blending ratio of 50%.[4,5] This Annex A5 fuel is produced by using an iso-butanol-to-jet pathway, and is mainly composed of isododecane (i-$C_{12}H_{26}$) and isocetane (i-$C_{16}H_{34}$), with mole fractions of about 83% and 17%, respectively.[4] Comprehensive understanding and modeling of combustion of AtJ-SPK and its blends with conventional Jet A fuel are essential for its efficient and clean utilization in the aircraft engines.

Regarding the combustion properties of AtJ-SPK and its blends with Jet A/Jet A-1, such as ignition delay time and laminar flame speed, there have been several experimental and kinetic modeling studies reported. Won et al.[8] experimentally measured the species profiles of AtJ-SPK global oxidization in a flow reactor, and compared the profiles with

those measured from other alternative jet fuels. Flora et al.[9] measured ignition properties of AtJ-SPK behind reflected waves from 980 K to 1980 K (ϕ = 0.5 and p = 16 atm), and made comparisons with other alternative jet and bio-jet fuels. Valco et al.[10] conducted the ignition delay measurements of AtJ-SPK at low temperatures from 625 K to 735 K (ϕ = 0.25, 0.5, and 1.0; p = 20 bar). Wang et al.[11] measured the ignition properties of AtJ-SPK and AtJ-SPK/Jet A blends (0, 20%, 50%, and 100%) from 1025 K to 1325 K (ϕ = 1.0 and p = 0.56 atm). They also measured laminar flame speeds of AtJ-SPK/air mixture ($0.8 \leqslant \phi \leqslant 1.4$ and T_u = 403 K). In terms of the kinetic modeling, they further extended the HyChem mechanism to model the combustion characteristics of pure AtJ-SPK (HyChem C1[12]) by assuming AtJ-SPK as a virtually-designed pure substances and combining the pyrolysis reactions and the subsequent oxidization reactions (updated version based on USC Mech II[13]). They also updated the HyChem C1 model by using optimized foundational fuel chemistry models to minimize the prediction uncertainties, and the underestimation of laminar flame speed under fuel-rich conditions has been improved.[14] Guzman et al.[15] experimentally measured the species profiles of AtJ-SPK in the pyrolytic and oxidative decomposition process (900 K $\leqslant T_{ini} \leqslant$ 1550 K and p = 4 bar), and they further validated the detailed kinetic model they developed by comparing the predicted species profiles with their measured data. Very recently, Richter et al.[4] experimentally studied the ignition properties of AtJ-SPK/air mixture from initial temperature of 850 K to 1700 K (ϕ = 1.0 and 2.0), and laminar flame speeds were also measured (T_u = 473 K, p = 1 and 3 bar, and $0.6 \leqslant \phi \leqslant 1.5$). In addition to the experiments, a new detailed mechanism was developed for the AtJ-SPK combustion, named LLNL-ATJ-SPK in the present study. This mechanism (LLNL-ATJ-SPK) was further validated by predicting the ignition and flame speeds under various conditions with the experimentally measured data as benchmarks.

The combustion characteristic of conventional Jet A fuel has been studied relatively much in many previous literature. In terms of the experimental approach, the ignition behavior[16–18] and laminar flame speeds[19,20] have been measured under various conditions. For the chemical

kinetic modeling of Jet A combustion, the fuel surrogate method was generally used.[17,21] In the fuel surrogates, several pure components are used to generally reproduce the combustion behavior and each component represents a certain type of the organic components. Several fuel surrogates and the corresponding detailed mechanisms have been developed, such as the POLIMI mechanism,[22] LLNL mechanism,[23] JetSurf2.0 mechanism,[24] and the detailed mechanism developed by Dooley et al.[21] For the details of the fuel surrogates and detailed kinetic mechanisms, interested readers can refer to Refs.[25,26] Furthermore, efforts have also been put into developing reduced mechanisms of jet fuels from those detailed mechanisms for computational fluid dynamic (CFD) simulations.[19,27,28] Recently, Wang et al.[11] extended their physics-based approach to Jet A fuel combustion modelling and developed a skeletal mechanism, HyChem A2 mechanism.[18] Regarding the combustion characteristics of AtJ-SPK/Jet A blends, only Wang et al.[29] reported the ignition behavior under various high temperatures and blending ratios, and laminar flame speeds were measured for AtJ-SPK and Jet A, respectively. In the aspect of kinetic modeling, they further employed the physics-based method for the modeling of AtJ-SPK/Jet A blends and developed the HyChem C1A2 (AtJ-SPK/Jet A blends) mechanism.[18]

Numerical simulation has proven to be an efficient tool for combustion research, in which the combustion chemistry plays a significant role. Among the above experimental and kinetic modeling studies, only HyChem C1[11,14] and LLNL-ATJ-SPK[4] mechanisms have been validated with their measured experimental data by calculating both the ignition delay times and laminar flame speeds. Very recently, Shastry et al.[28] developed the analytically reduced chemistry for AtJ-SPK and Jet A-1, respectively, from the POLIMI detailed mechanism.[22] They partially validated the chemistry under limited conditions (ϕ = 0.6 - 2.0, T_u = 450 K, and 1 bar for laminar flame speed; T_{ini} = 1000.0 - 2400 K, p = 1 bar, and ϕ = 1.0 for ignition delay), by comparing with the POLIMI mechanism predictions. However, the performance of their developed reduced chemistry on various initial temperatures, pressures, and AtJ-SPK/Jet A-1 blending ratios was not accessed. For the AtJ-SPK/Jet A blends, only

the HyChem C1/A2 mechanism[30] was developed and validated with the experimental data under limited conditions.[11] As found in our previous study,[31] the evaporation rate of each component in the multi-component fuel is different from each other, which has also been proven to considerably affect the flame structure and auto-ignition behavior.[32,33] On the one hand, although HyChem C1[12] and C1A2[30] mechanisms can consider the actual distillation curve of the liquid fuel and fuel blends,[34] this kind of non-uniform evaporation effect could not be explicitly reflected as AtJ-SPK and Jet A are considered as virtual pure substances in the implementation. On the other hand, those detailed mechanisms developed based on the fuel surrogate method, such as LLNL-AtJ-SPK and POLIMI detailed mechanisms, can explicitly consider this effect, but their sizes are very large for Computational Fluid Dynamics (CFD) and make them very hard and almost impossible to use, particularly in the three-dimensional (3D) CFD calculations.

To address this issue, the present study aims to develop reduced mechanisms for AtJ-SPK and its blends with Jet A from the LLNL-AtJ-SPK[4] and POLIMI detailed mechanisms[22], respectively, which can explicitly consider the non-uniform evaporation effect. The Directed Relation Graph (DRG) with Error Propagation (DRGEP),[35] Directed Relation Graph with Path Flux Analysis (DRGPFA),[36] and Full-Species Sensitivity Analysis (FSSA)[37] methods are used sequentially during the reduction process. The developed reduced mechanisms are further validated by comparing the predicted ignition delay, laminar flame speed, and temporal/spatial profiles with those of the master detailed mechanisms and the experimentally measured data. Finally, the computational costs of the reduced and master mechanisms are also compared and discussed in different dimensions of calculation.

The remaining of this paper is organized as follows. Section 2 describes the development procedures of the reduced mechanisms. Section 3 comprehensively validates the accuracy of the developed reduced mechanisms. Section 4 discusses the computational cost in different dimensions of calculation. The final section provides concluding remarks.

2 Mechanism reduction processes

In the present work, two reduced mechanisms are developed for pure AtJ-SPK and AtJ-SPK/Jet A blends, respectively. For pure AtJ-SPK combustion, the reduced mechanism is developed from the LLNL-ATJ-SPK detailed mechanism[4] since this detailed mechanism was proven to perform well at various conditions. However, the species in the commonly used fuel surrogate of Jet A (N-$C_{12}H_{26}$, I-C_8H_{18} and C_8H_{10}[38,39]) are not included. Therefore, it can not be used for AtJ-SPK/Jet A blends. Therefore, the reduced mechanism for AtJ-SPK/Jet A blends is developed from the POLIMI detailed mechanism.[22] This choice is made based on the following two considerations. The first consideration is that both the multiple fuel components, AtJ-SPK (17% I-$C_{16}H_{34}$ and 83% I-$C_{12}H_{26}$)[4] and Jet A (37% N-$C_{12}H_{26}$, 27.5% I-C_8H_{18}, and 35.5% C_8H_{10}[38,39]), are included in this mechanism. The second consideration is that this mechanism can give acceptable predictions on ignition delay times and laminar flame speeds for AtJ-SPK and Jet A under various conditions (see the supporting information). However, its accuracy is relatively worse than that of the LLNL-AtJ-SPK detailed mechanism for pure AtJ-SPK fuel, especially at the relatively low fresh temperature (see the supporting information). Therefore, LLNL-ATJ-SPK and POLIMI detailed mechanisms are selected as the master mechanisms for AtJ-SPK and its blends with Jet A, respectively.

The DRGEP,[35] DRGPFA[36] and FSSA[37] methods are used sequentially in the development of the reduced mechanism as shown in Figure 1. The DRGEP method achieves the mechanism reduction through measuring the error propagation from the species removal and the related reactions down graph pathways. Pepiot and Pitsch proposed this method[35] based on the original DRG method developed by Lu and Law[40] and has been successfully adopted in many previous studies.[41–43] Sun et al.[36] proposed the DRGPFA method based on the DRG method. The difference compared with DRGEP is that it defines the directed graph and measures the species importance through considering both the production and consumption

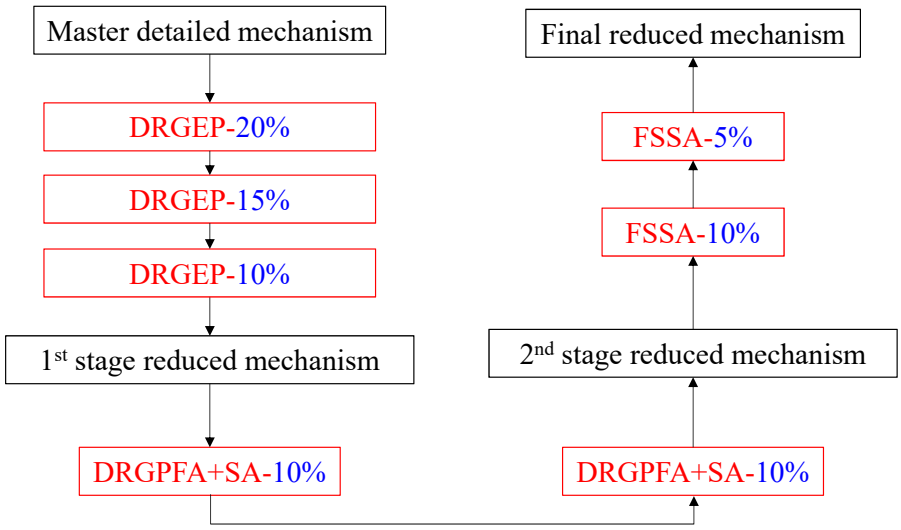

Figure 1: Schematic diagram of the mechanism reduction processes

fluxes. This method has also been successfully employed for mechanism reduction in many previous studies.[44,45] FSSA[37] is more effective in analyzing the species importance in the whole reaction kinetics, but it is very time-consuming. Therefore, it is used in the final stage when the numbers of species and reactions are relatively smaller after the reductions using DRGEP and DRGPFA methods. The details of those methods are not detailed here for brevity; interested readers can refer to Refs.[35–37] In the first stage, three steps of DRGEP reduction are initially used to remove species and irrelevant reactions, and the error tolerance in each step gradually decreases from 20% to 10%. In the second stage, two steps of DRGPFA+SA reduction are used, and the error tolerances are set as 10%. Finally, after the reductions of DRGEP and DRGPFA, two steps of FSSA reduction are conducted with the error tolerances of 10% and 5%, respectively. During the reduction process, the error tolerance is gradually decreased from 20% to 5%. This is used to avoid significant deviation growth in the multiple reduction steps.

In the reduction of LLNL-AtJ-SPK detailed mechanism, ignition delay times and mole fractions of I-$C_{12}H_{26}$ ($XC_{12}H_{26}$), I-$C_{16}H_{34}$ (HMN), O_2, N_2, CO_2, I-C_4H_8, and H_2O are set as the targets, and the operation conditions cover wide ranges of initial temperature (800 - 1600 K; interval: 100 K), equivalence ratio (0.6 - 1.6; interval: 0.1), and pressure (1, 10,

and 20 atm). Note that isobutene (I-C_4H_8) is also included as it was proven to be the major intermediate species during pyrolysis and oxidization processes of the highly branched fuels.[4] The ignition delay times and temporal profiles of those interested species are obtained from the temporal evolution of the zero-dimensional (0D) homogeneous reactor using CHEMKIN-PRO.[46] The number of species/reactions and error-related parameters of each step in the reduction process are listed in Table 1. The mechanism size can be reduced to 385 species and 2011 reactions after three steps of DRGEP reductions, and further to 222 species and 1142 reactions after two steps of DRGPFA reduction. The final reduced mechanism, containing 149 species and 732 reactions, could be obtained after two steps of FSSA reduction (see the supporting information for its CHEMKIN, OpenFOAM, and Cantera formats).

Table 1: Error-related parameters and mechanism size in reduction process of the LLNL-AtJ-SPK detailed mechanism.

Step	Methods	Error tolerance [-]	Number of species [-]	Number of reactions [-]	Max. error percentage [-]
0	-	-	1832	7337	-
1	DRGEP	20%	673	3155	95.70%
2	DRGEP	15%	470	2317	76.60%
3	DRGEP	10%	385	2011	24.30%
4	DRGPFA+SA	10%	333	1766	79.40%
5	DRGPFA+SA	10%	222	1142	96.60%
6	FSSA	10%	188	922	76.10%
7	FSSA	5%	149	732	62.80%

As for the POLIMI detailed mechanism, the reduction processes are also conducted based on the temporal evolution of 0D homogeneous reactor using CHEMKIN-PRO.[46] Ignition delay times and mole fractions of AtJ-SPK components (I-$C_{16}H_{34}$ and I-$C_{12}H_{26}$), Jet A components (N-$C_{12}H_{26}$, I-C_8H_{18}, and C_8H_{10}), O_2, N_2, H_2O, CO_2, C_2H_4, and I-C_4H_8 are set as the targets for error tolerance checks. Note that C_2H_4 and I-C_4H_8 are considered here because they have been found to be the important products of the pyrolysis reactions of Jet A and AtJ-SPK fuels, respectively.[4,29] The operation conditions consider a wide range of initial temperatures (800 to 1600 K, interval: 200 K), equivalence ratios (0.6 to 1.6, interval: 0.2), pressures (1, 10,and 20 atm), and blending ratios (BR: 0, 0.2, 0.5, and 1.0). Here,

BR represents the AtJ-SPK fraction in the fuel stream. The total case number is 360, and all of the conditions are used in each reduction step. Table 2 lists the size of the obtained reduced mechanisms and the error-related parameters (error tolerance and maximum error percentage) in each step. Starting from the master mechanism, the mechanism size can be reduced to 225 species and 6576 reactions, respectively, after three DRGEP reduction processes. Then, the mechanism size can be further reduced to 164 species and 3288 reactions after two DRGPFA+SA reductions. Finally, the final reduced mechanism has 75 species and 1099 reactions after two FSSA reduction processes (see the supporting information for its CHEMKIN, OpenFOAM, and Cantera formats).

Table 2: Error-related parameters and mechanism size in reduction process of the POLIMI detailed mechanism.

Step	Methods	Error tolerance [-]	Number of species [-]	Number of reactions [-]	Max. error percentage [-]
0	-	-	368	14462	-
1	DRGEP	20%	254	8092	45.40%
2	DRGEP	15%	229	6650	95.40%
3	DRGEP	10%	225	6576	69.67%
4	DRGPFA+SA	10%	180	3974	79.40%
5	DRGPFA+SA	10%	164	3288	96.60%
6	FSSA	10%	101	1485	76.20%
7	FSSA	5%	75	1099	84.60%

3 Validation of the reduced mechanisms

The developed reduced mechanisms for pure AtJ-SPK and AtJ-SPK blends are validated by comparing the predicted ignition delay, laminar flame speed, and temporal/spatial profiles with those predicting using the master detailed mechanisms as well as experimental data.

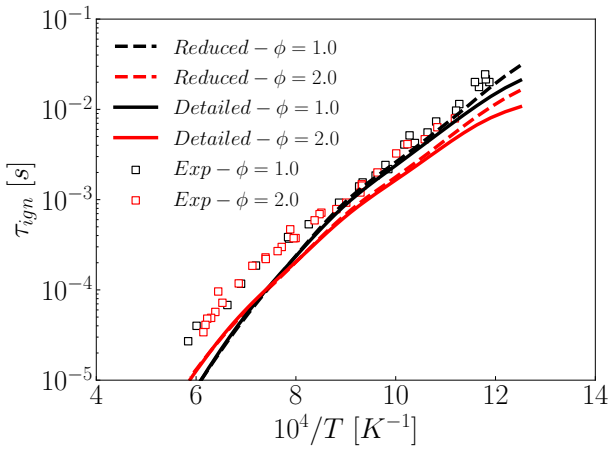

Figure 2: Ignition delay times measured from the experiment[4] and predicted by the LLNL-AtJ-SPK mechanism and the developed reduced mechanism (p_{ini} = 16 bar; ϕ =1.0 and 2.0; T_{ini} = 800 K - 1700 K). Note that the pressure profile measured in the experiment (provided by the supplementary materials of Ref.[4]) is used in all the calculations.

3.1 Reduced mechanism for pure AtJ-SPK

3.1.1 Ignition delay

Figure 2 demonstrates comparisons of ignition delay times measured in the experiment[4] and predicted using the LLNL-AtJ-SPK and reduced mechanisms. Note that pressure of the reaction system is initially 16 bar and varies with time (the values are directly obtained from the supplementary materials of Ref.[4]). The 'OH' species is used to reflect the ignition signal, which is different from the 'CH*' signal used in the experiments. This is also the reason why the present predictions are slightly different from those in Ref.[4] Selecting 'OH' as the ignition signal species considers the following reasons: 1) 'CH*' species is removed from the LLNL-AtJ-SPK mechanism in the reduction process (excluded in the reduced mechanism), therefore it is technically impossible to use this species as the ignition signal for a consistent comparison; 2) 'OH' is included in both the reduced and LLNL-AtJ-SPK mechanisms and has been widely used as an indicator of ignition signal in many previous studies.[47–49] Overall, the ignition behavior at different temperatures measured in the experiments under stoichiometric and rich conditions could be well reproduced by both the LLNL-AtJ-SPK and

reduced mechanisms. Future efforts might be needed to mild optimize kinetic parameters to eliminate the slight discrepancy at high-temperature conditions. At high temperatures, the reduced mechanism could give almost the same predictions as those of the LLNL-AtJ-SPK mechanism. Whereas, at relatively lower temperatures ($T_u < 900$ K), the reduced mechanism slightly over-estimates the ignition delay times. This might be related to the removal of some complicated low temperature reactions during the reduction process.

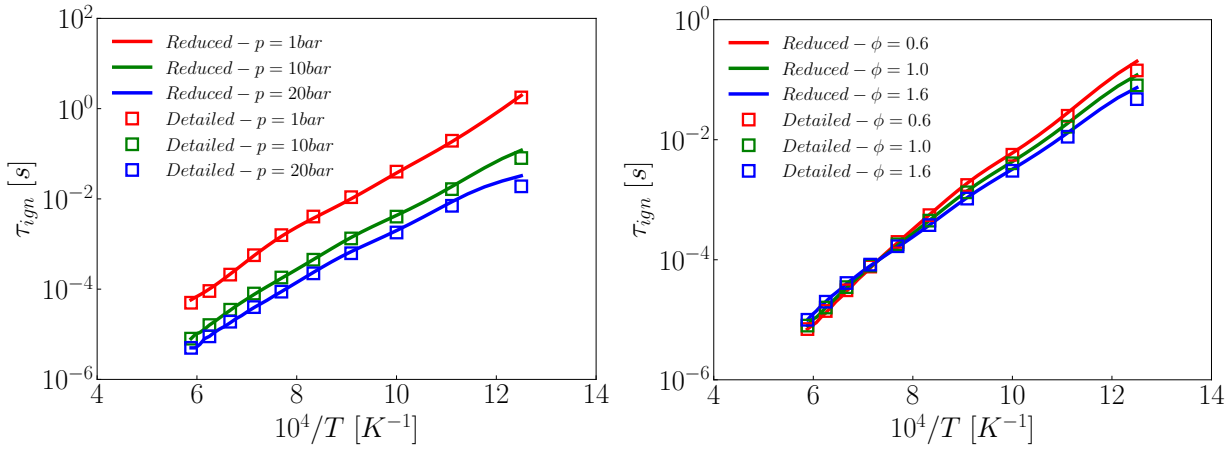

Figure 3: Comparison of the ignition delay times calculated using the LLNL-AtJ-SPK and reduced mechanisms (T_{ini} = 800 K - 1700 K): Left: different pressures (ϕ = 1.0); Right: different equivalence ratios (p = 10 bar).

The reduced mechanism is used to calculate the ignition delay times of AtJ-SPK under various conditions to further validate its accuracy. Because the experimental data is not available for these conditions, here the comparisons are only conducted between the predictions of the reduced and LLNL-AtJ-SPK mechanisms as shown in Figure 3. It is found that pressure has a more profound effect on ignition delay time than that of equivalence ratio. The reduced mechanism can well reproduce the the LLNL-AtJ-SPK mechanism predictions at 1 bar; in particular, the low temperature chemical effect can be well captured. With an increase of pressure, the accuracy is slightly decreased at the low temperature regions (overestimates the ignition delay times at $T_u < 900$ K). The effect of equivalence ratio can also be well represented. Specifically, ignition delay times under lean-/stoichiometric-/rich- conditions can be well reproduced by the reduced mechanism. Overall, the developed

reduced mechanism can well describe the ignition behavior of AtJ-SPK under various conditions, showing very good agreements with the LLNL-AtJ-SPK mechanism predictions and experimental data.

3.1.2 Temporal profiles

The reaction mechanism describes the nonlinear reacting characteristics of the complicated multi-components in the reaction system. Temporal profiles of temperature and species in the system are also of great interest for validation of the developed reduced mechanism. Figure 4 demonstrates temporal profiles of gas temperature and mass fractions of major/minor species predicted by the developed reduced (solid lines) and LLNL-AtJ-SPK (scatters) mechanisms at various initial temperatures and equivalence ratios. These species include the AtJ-SPK fuel components, major products (CO_2 and H_2O), and minor intermediate species (OH and CO). Five initial temperatures (800, 1000, 1200, 1400, and 1600 K) and stoichiometric/rich conditions ($\phi = 1.0$ and 2.0) are considered, and the pressure is 1 bar. Under the stoichiometric condition (see Figure 4(a)), all the temporal profiles agree well with the LLNL-AtJ-SPK mechanism predictions when initial temperature is above 1000 K. However, at $T_{ini} = 800$ K, all the predicted profiles are slightly delayed compared with those of the LLNL-AtJ-SPK mechanism. This is consistent with the slight overestimation as shown in Figures 2 and 3. Even with slight delays, the overall temporal evolution trends and values could be accurately reproduced by the developed reduced mechanism. As for the fuel-rich condition ($\phi = 2.0$, see Figure 4(b)), the reduced mechanism also could well reproduce the LLNL-AtJ-SPK mechanism predictions with high accuracy. Note that major products (CO_2 and H_2O) profiles show a slightly different trend from that at stoichiometric condition. Specifically, their mass fractions would slightly decrease over time. This difference could also be accurately reproduced using the reduced mechanism.

Under various pressures from the atmospheric condition (1 bar) to the operating condition of the realistic aircraft engine (20 bar),[50,51] comparisons between the predictions of the

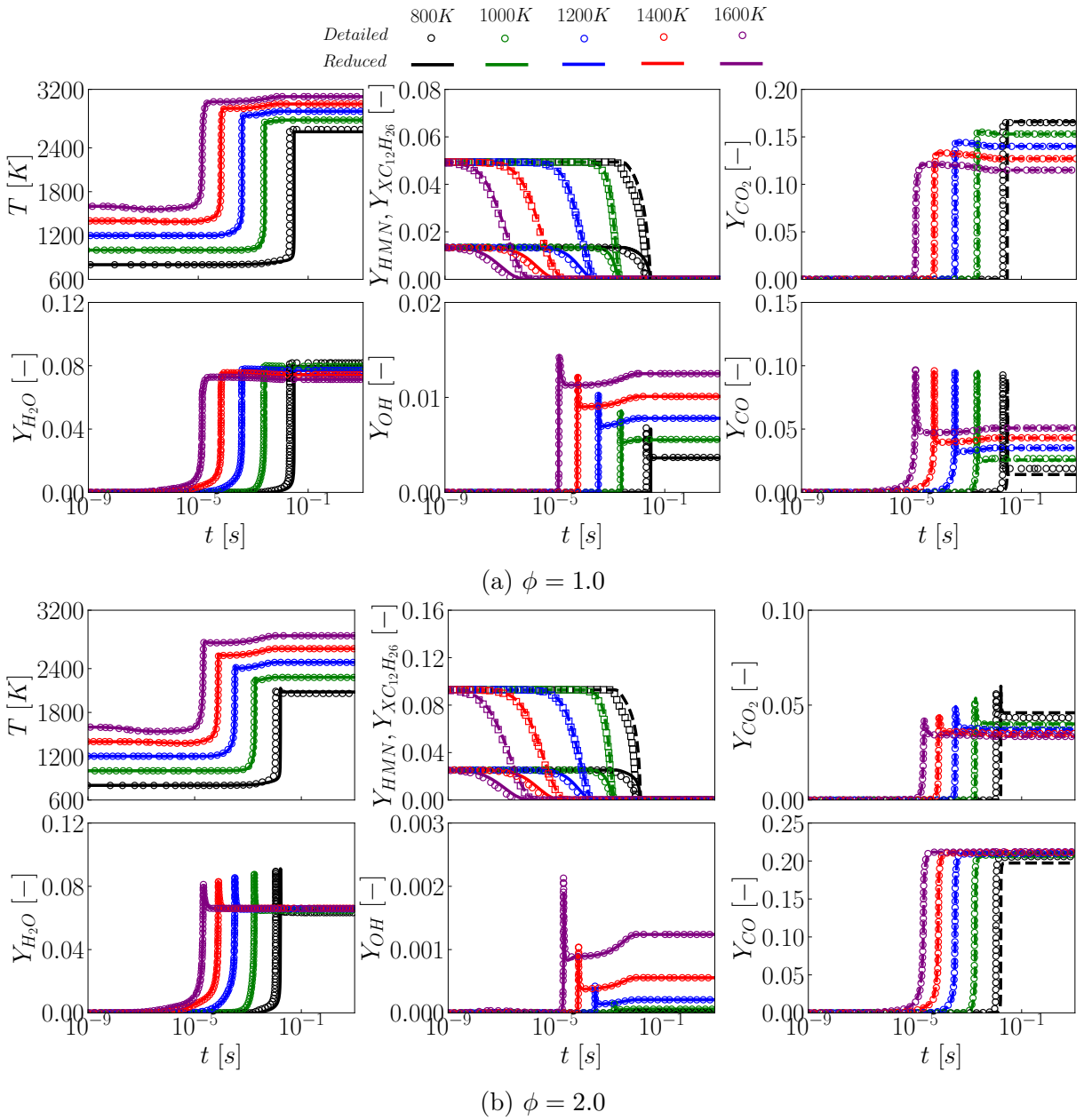

Figure 4: Comparisons of the temporal profiles of gas temperature, and mass fraction of major species and minor species (HMN, $XC_{12}HC_{26}$, CO_2, H_2O, CO, CO_2, and OH) predicted by the LLNL-AtJ-SPK and reduced mechanisms under various initial temperatures (800 K to 1600 K) and equivalence ratios: (a) ϕ=1.0; (b) ϕ=2.0. The operation pressure is 1 bar.

reduced and LLNL-AtJ-SPK mechanisms are shown in Fig. 5. The figure legend is the same as that in Figure 4. Overall, the reduced mechanism performs well in reproducing the temporal evolution of the reaction system at various pressures and initial temperatures. It should be noted that the accuracy slightly decreases but remains at a high level as pressure

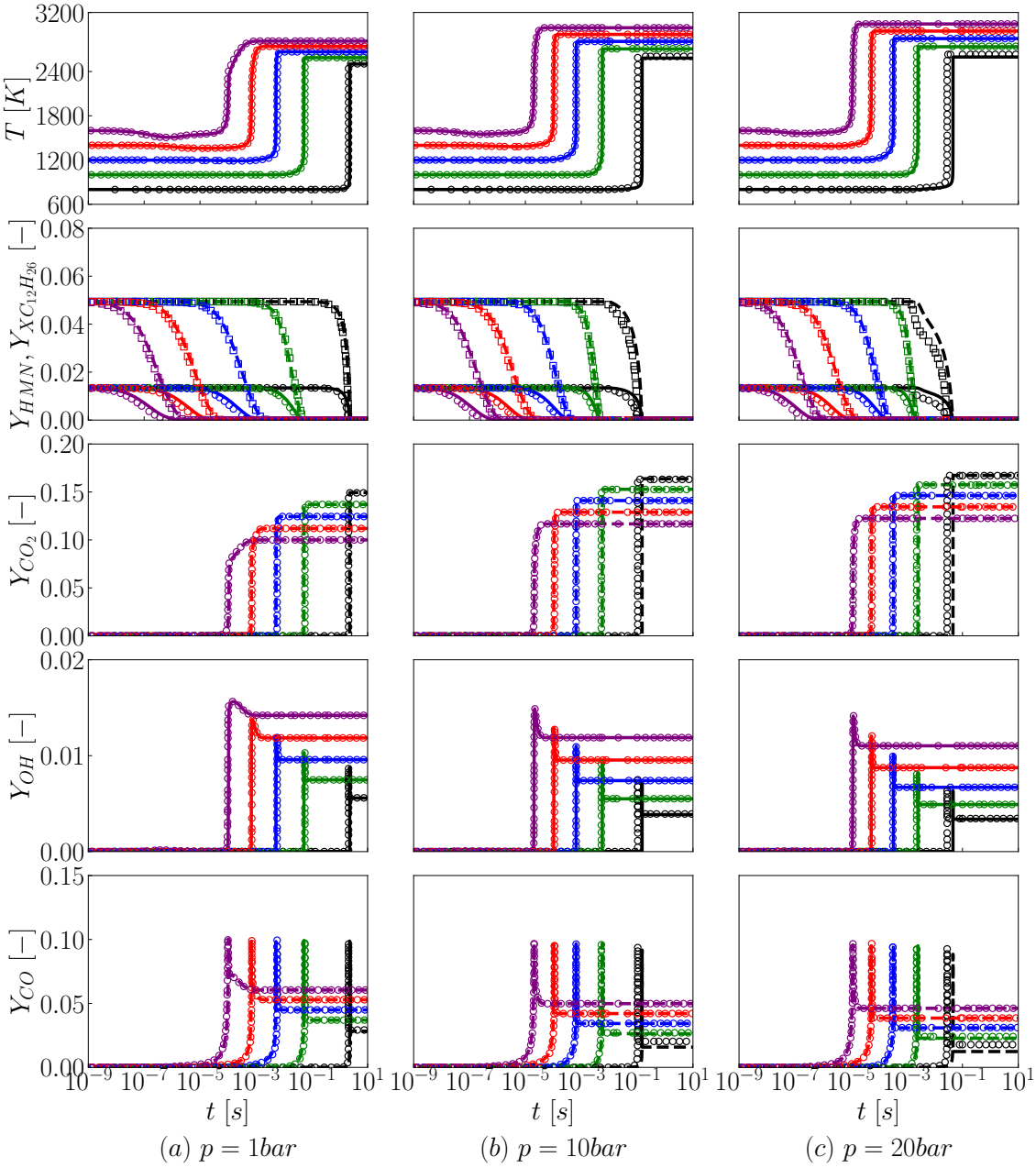

Figure 5: Temporal profiles of temperature and mass fractions of major species/minor species predicted using the LLNL-AtJ-SPK and reduced mechanisms under various temperatures and pressures ($\phi = 1.0$): (a) $p = 1$ bar; (b) $p = 10$ bar; (c) $p = 20$ bar. The legend is the same as that of Figure 4.

increases, which is consistent with predictions as shown in Figure 3(a).

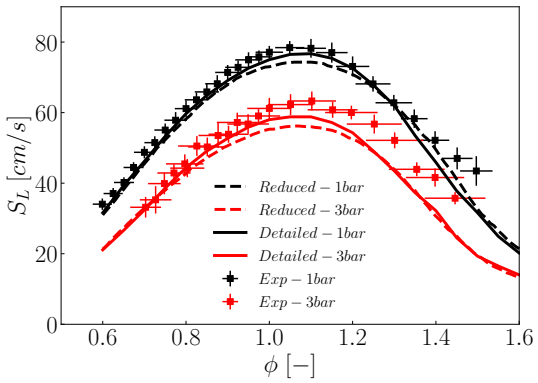

Figure 6: Comparisons of laminar flame speeds measured in the experiment[4] and calculated using the LLNL-AtJ-SPK and reduced mechanisms under different equivalence ratios (0.6 - 1.6) and pressures (1 and 3 bar).

3.1.3 Laminar flame speed

Laminar flame speed is also an important fuel combustion properties of great interest. In this part, the developed reduced mechanism is employed to calculate laminar flame speeds under various conditions by calculating one-dimensional (1D) freely propagating premixed flames, comparing with the LLNL-AtJ-SPK mechanism predictions and the experimental data.[4] Figure 6 demonstrates laminar flame speeds measured in the experiments[4] and predicted using the LLNL-AtJ-SPK and reduced mechanisms under various equivalence ratios (0.6 - 1.6) and two pressures (1 and 3 bar). The experimental data and uncertainties are obtained from the supplementary materials of Ref.[4] Overall, the reduced mechanism could well reproduce laminar flame speeds predicted by the LLNL-AtJ-SPK mechanism and measured in the experimental data. Specifically, compared with the experimental data, both reduced and LLNL-AtJ-SPK mechanisms could accurately reproduce the behaviors at lean conditions. Under stoichiometric and rich conditions, the experimental data could be accurately well reproduced at 1 bar but slightly under-estimated at 3 bar. This is consistent with the study of Richter et al.[4] As for the comparisons between predictions of reduced and LLNL-AtJ-SPK mechanisms, their results almost coincide at lean and rich conditions. However, under equivalence ratios near the stoichiometric condition, the reduced mechanism slightly underestimates laminar flame speeds, and the discrepancies are less than 8 %. More com-

parisons under various unburnt temperatures, pressures, and equivalence ratios are shown in Figure 7. The reduced mechanism predictions are also in very good agreements with the

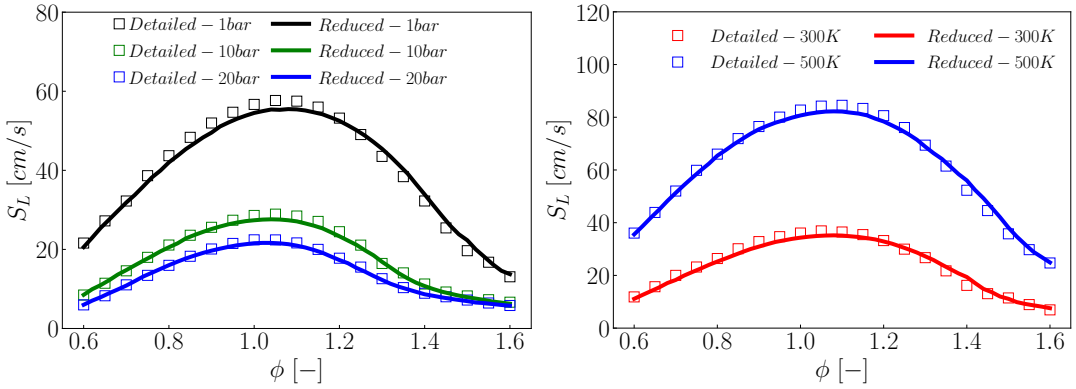

Figure 7: Comparisons of laminar flame speeds predicted by the LLNL-AtJ-SPK mechanism and developed reduced mechanism for various conditions (ϕ = 0.6 - 1.6): Left: different pressures (T_u = 400 K); Right: different fresh fuel/air mixture temperatures (p = 1 bar).

LLNL-AtJ-SPK mechanism predictions, although there are still slight discrepancies near the stoichiometric condition. The above analyses and comparisons indicate that the effects of pressure, unburnt mixture temperature, and equivalence ratio can be well represented using the developed reduced mechanism.

3.1.4 Spatial profiles

The 1D freely propagating premixed flames can be used not only for laminar flame speed calculations but also to construct the flamelet tables when using the Flamelet Generated Manifold method.[52–54] The spatial profiles of the 1D freely propagating premixed flames are also of interest to further explore the potential of this reduced mechanism in turbulent combustion simulations. Therefore, the spatial profiles calculated using the reduced and LLNL-AtJ-SPK mechanisms under various conditions are further compared. Figure 8 shows comparisons under various pressures, and Figure 9 demonstrates comparisons under various T_u values and equivalence ratios. Note that only regions of interest in the whole computational domain are shown and OH mole fractions are timed to several times for a clearer observation. The flame structures predicted using the LLNL-AtJ-SPK mechanism can be

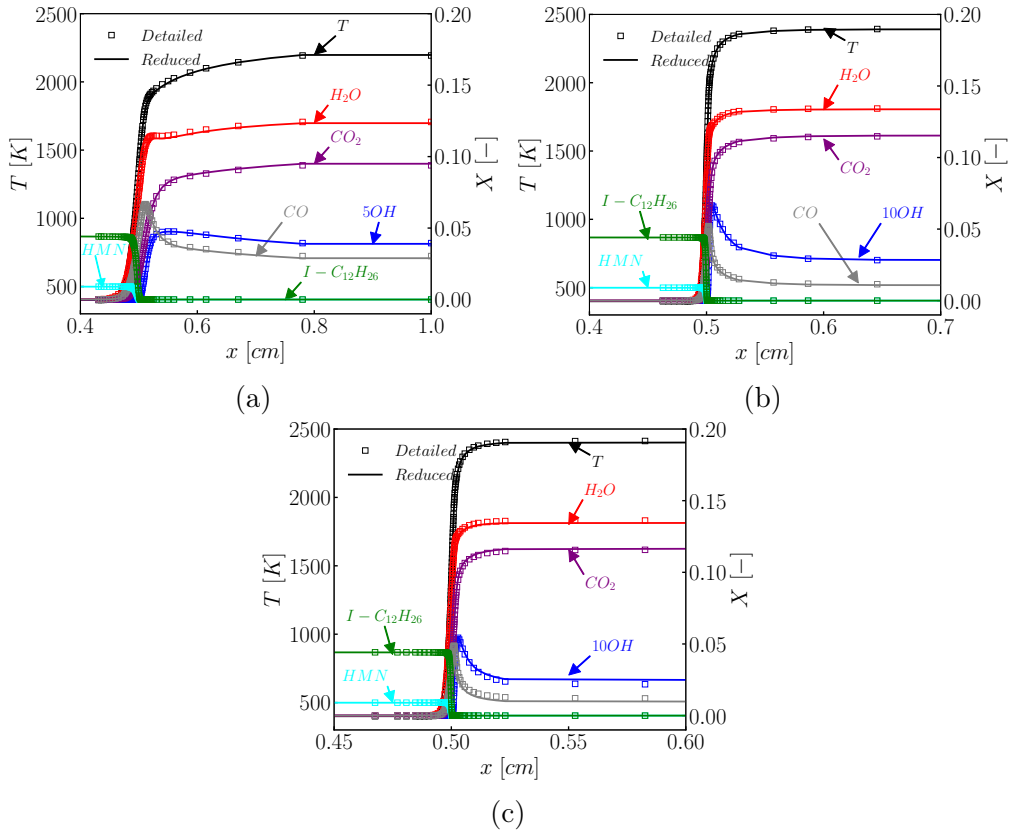

Figure 8: Comparisons of temperature and major/minor species profiles calculated using the LLNL-AtJ-SPK and reduced mechanisms under various pressures ($\phi = 1.0$, $T_u = 400$ K): (a) $p = 1$ bar; (b) $p = 10$ bar; (c) $p = 20$ bar.

well reproduced by the reduced mechanism under various pressures, equivalence ratios and unburnt temperatures. Especially, spatial profiles of temperature and mole fractions of the major/minor species almost coincide, even for the minor intermediate species OH and CO.

3.2 Reduced mechanism for AtJ-SPK/Jet A blends

3.2.1 Ignition delay

Figure 10 demonstrates ignition delay times predicted using the developed reduced and POLIMI mechanisms under various conditions. Under lean-/stoichiometric-/rich- conditions, the reduced mechanism performs well at high temperatures but slightly overestimates at relatively low temperatures as shown in Figure 10(a). The developed reduced mechanism

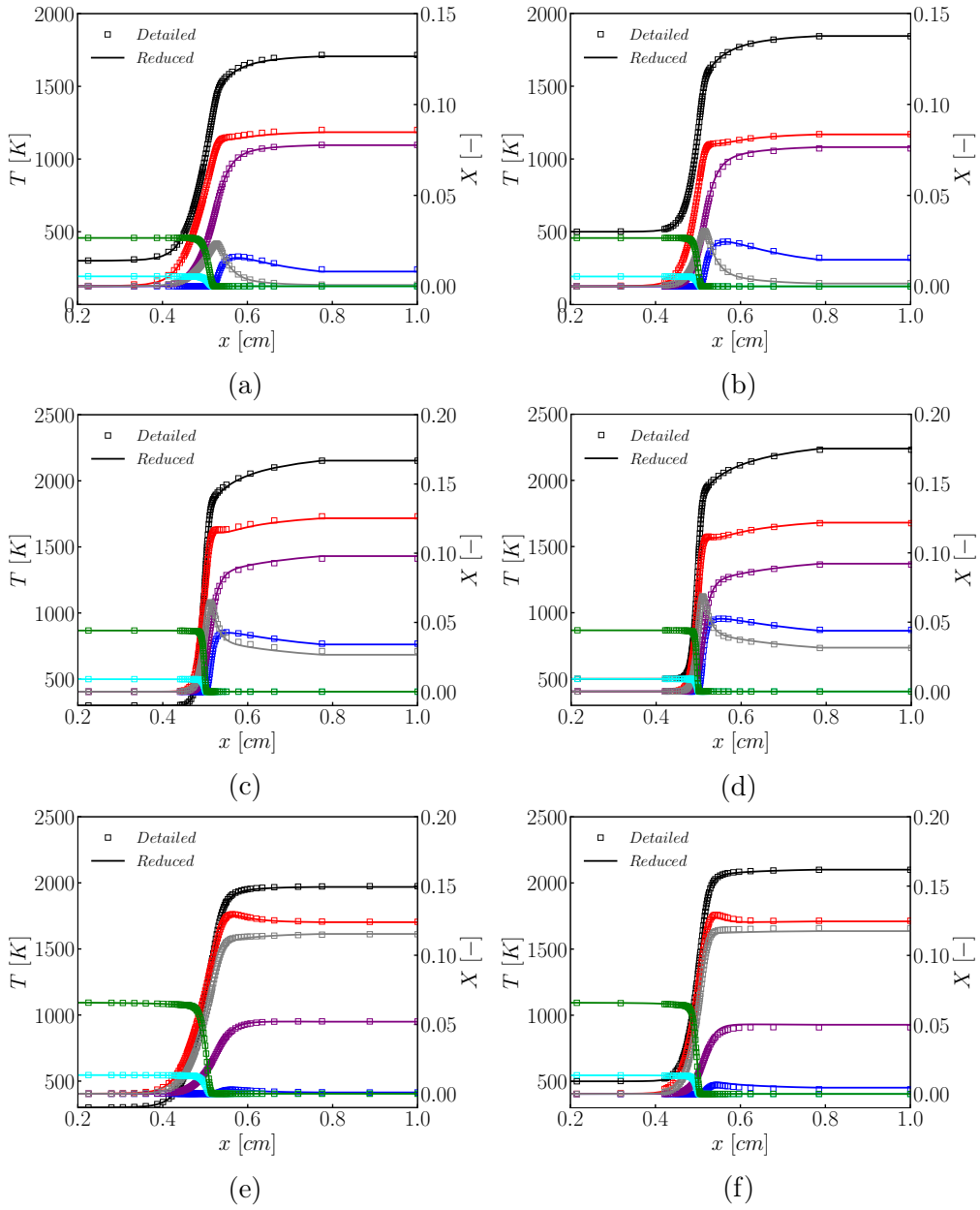

Figure 9: Comparisons of temperature and major/minor species profiles calculated using the LLNL-AtJ-SPK and reduced mechanisms under various various unburnt temperatures (300 K and 500 K) and equivalence ratios (p = 1 bar). (a,c,e) ϕ = 0.6, 1.0, and 1.6 (p = 1 bar, T_u = 300 K); (b,d,f) ϕ = 0.6, 1.0, and 1.6 (p = 1 bar, T_u = 500 K). The colors for species are the same as those of Figure 8.

can also reproduce the ignition behavior for conditions with various blending ratios as shown in Figure 10(b), and the slight deviations at low temperatures still remain, even for pure AtJ-SPK. At the atmosphere condition, the developed reduced mechanism can well reproduce

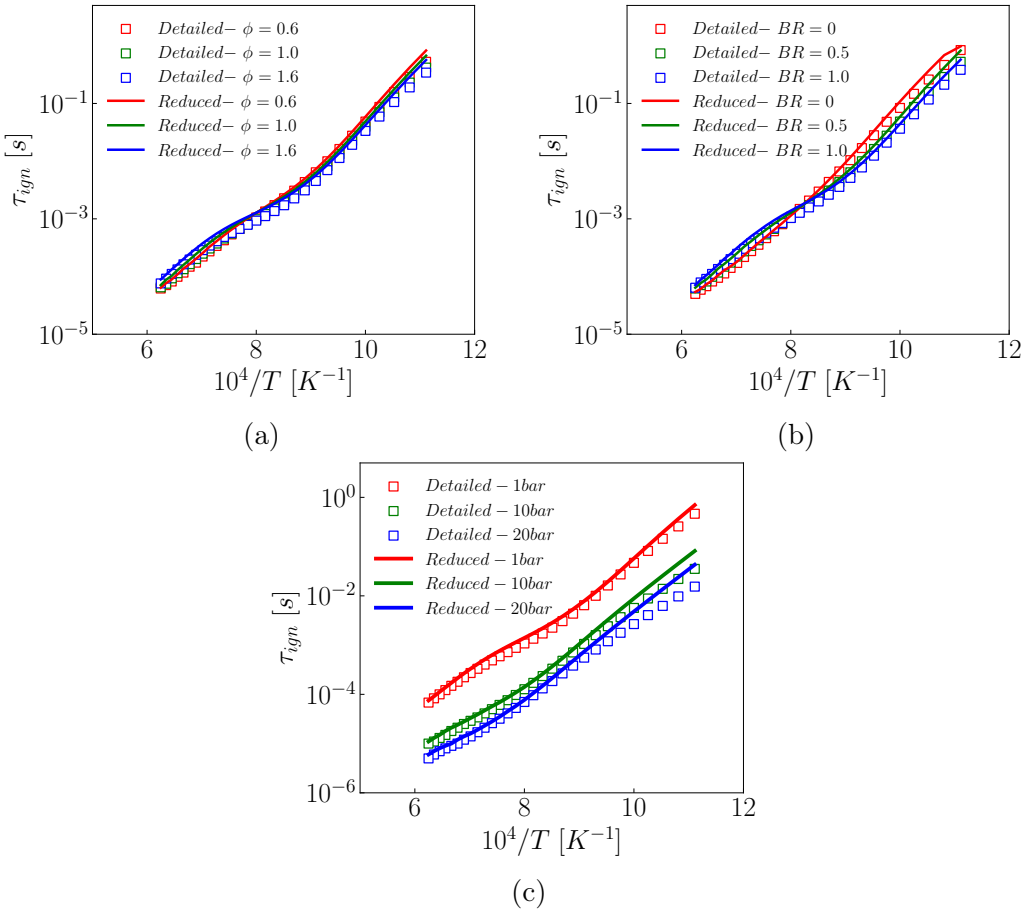

Figure 10: Ignition delay times calculated using the reduced and POLIMI mechanisms: (a) different ϕ, BR = 0.5, and p = 10 bar, (b) different BRs, ϕ = 1.0, and p = 1 bar, and (c) different pressures, ϕ = 1.0, and BR = 0.2.

the ignition behavior at both low and high temperatures, as shown in Figure 10(c). However, with the increasing of pressure, the ignition delay times are overestimated at low temperature conditions, in particular at $T_{ini} < 1000$ K. This might be attributed to that some pressure-dependent reactions are removed in the reduction process. Overall, the developed reduced mechanism can well reproduce the ignition delay predictions of POLIMI mechanism under various conditions with slight deviations at low temperatures.

3.2.2 Temporal profiles

Figure 11 demonstrates the temporal profiles of gas temperature and major/minor species of 0D reaction systems predicted by the reduced and POLIMI mechanisms under various initial

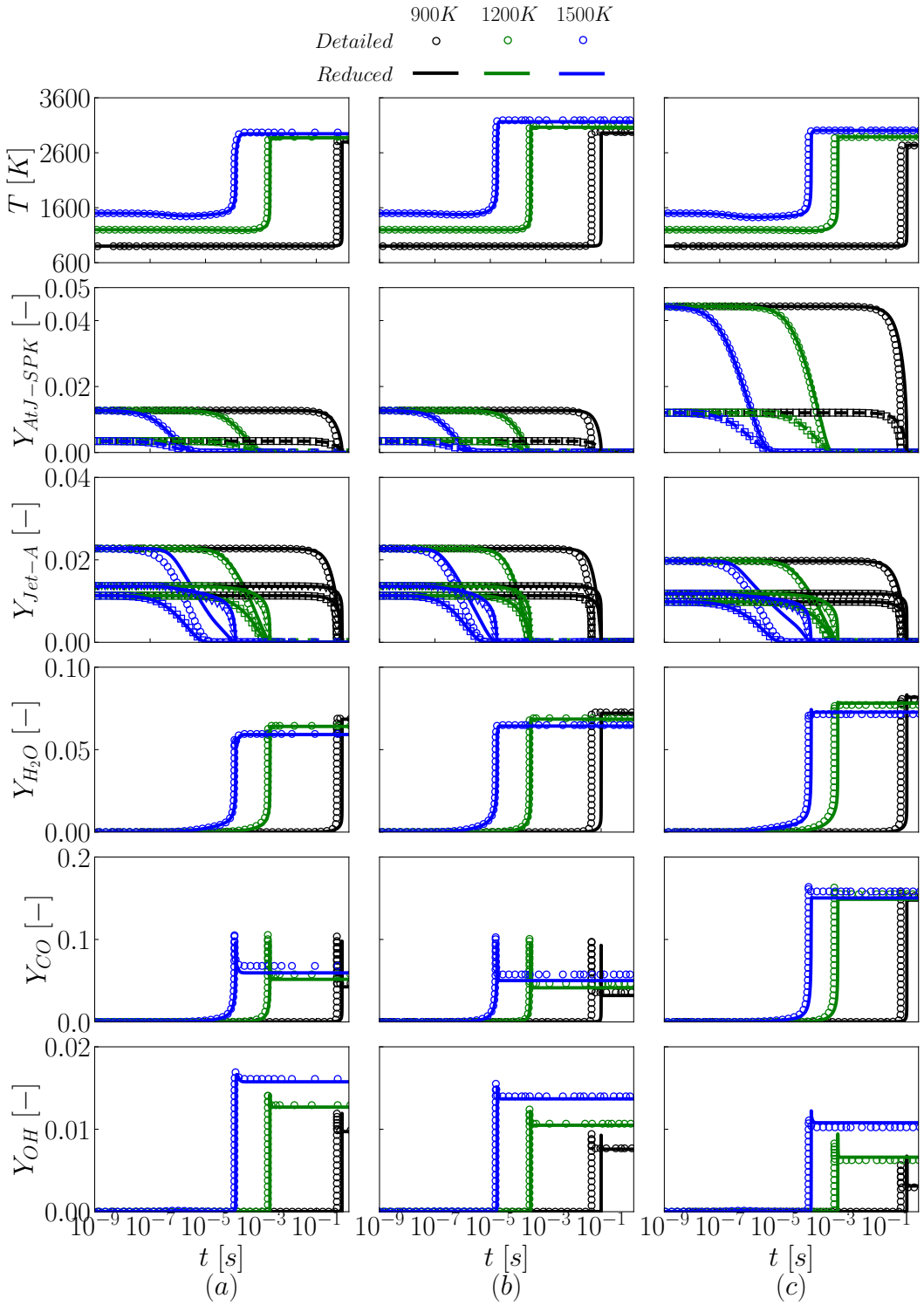

Figure 11: Temporal profiles of temperature and major/minor species predicted using the POLIMI and reduced mechanisms under various initial temperatures (900, 1200, and 1500 K): (a) ϕ = 1.0, p = 1 bar, and BR = 0.2, (b) ϕ = 1.0, p = 10 bar, and BR = 0.2, (c) ϕ = 1.6, p = 1 bar, and BR = 0.5.

temperatures (ϕ = 1.0, p = 1 bar, and BR = 0.2). Note that for the species profiles, only the fuel species, one product (H_2O), and two intermediate minor species are shown here for brevity. For the temperature profiles, the reduced mechanism can well reproduce the POLIMI mechanism predictions at high initial temperatures (T_{ini} = 1200 and 1500 K). However, there is a slight delay when the initial temperature is less than 900 K, which is consistent with the overestimation trend in Figure 10. For the AtJ-SPK fuel species, the developed reduced mechanism performs well at all the three temperatures. For I-C_8H_{18} and C_8H_{10} in the Jet A fuel surrogate, the reduced mechanism can accurately reproduce the temporal profiles. However, at T_{ini} = 1500 K, the consumption rate of N-$C_{12}H_{26}$ is underestimated. It is also interesting to find that the predicted temperature and other species profiles do not show obvious deviations compared with the POLIMI mechanism predictions. The H_2O profiles can be reproduced well with a slight delay at T_{ini} = 900 K, and OH profiles show a similar trend. The CO profiles first increase sharply and then decrease due to consumption, which can well captured by the reduced mechanism. However, the final CO mass fractions are slightly underestimated.

3.2.3 Laminar flame speed

For experimental measurements of laminar flame speeds of pure AtJ-SPK and Jet A, there have been several studies reported.[19,20,29] However, there have been none reports for measurements of AtJ-SPK/Jet A blends. The detailed POLIMI mechanism can generally reproduce laminar flame speeds of pure AtJ-SPK and Jet A under various conditions (see the supporting information). Therefore, the predictions of the POLIMI detailed mechanism are used as the benchmarks for validation of the developed reduced mechanism in the following comparisons.

Figure 12 compares laminar flame speeds calculated using the reduced and POLIMI mechanisms under various equivalence ratios, pressures, unburnt temperatures, and blending ratios. Under different unburnt temperatures, the laminar flame speed increases as the

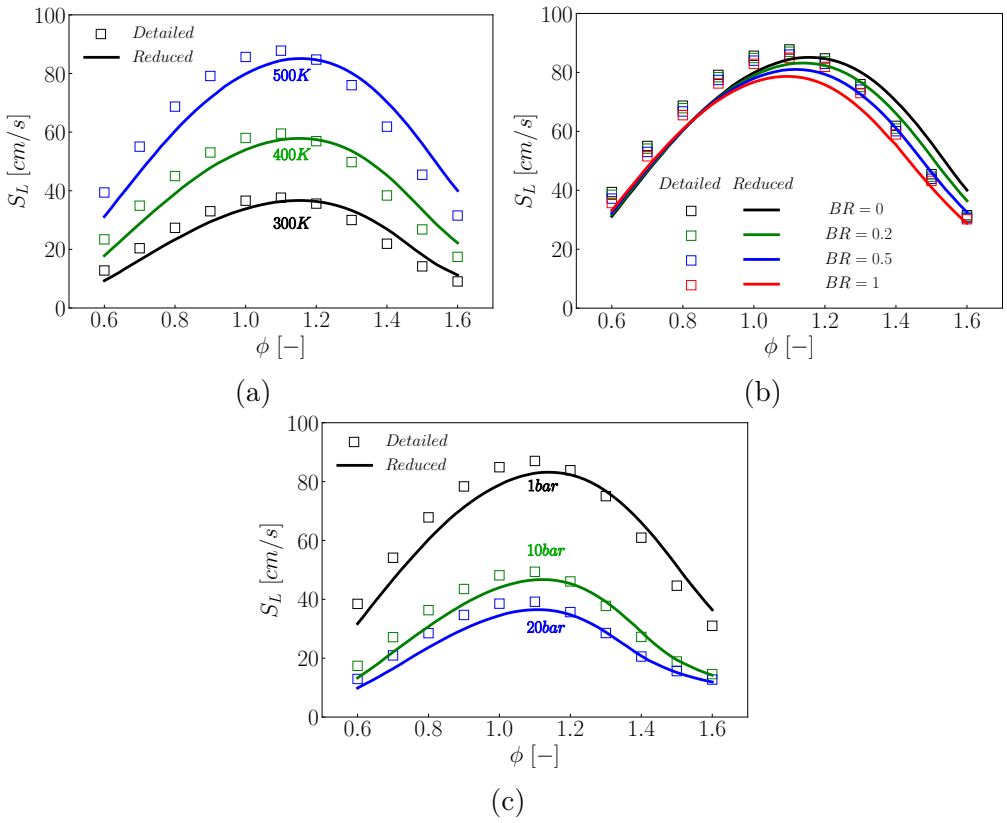

Figure 12: Laminar flame speeds predicted by the reduced and POLIMI mechanisms under various conditions: (a) different T_{ini}, BR = 0.0, p = 1 bar; (b) different BRs, T_{ini} = 500 K, p = 1 bar; (c) different pressures, T_{ini} = 500 K, BR = 0.2

unburnt temperature increases, and the peak value locates at ϕ=1.1 as shown in Fig. 12(a). This can be captured by the reduced mechanism. However, laminar flame speeds are slightly underestimated under lean conditions and overestimated under rich conditions, and the relative errors are less than 20%. With the increasing of blending ratio, laminar flame speeds predicted using the POLIMI mechanism slightly increase under lean-/stoichiometric-/rich-conditions as shown in Fig. 12(b). This can not be fully reproduced by the reduced mechanism. Specifically, laminar flame speeds predicted using the developed reduced mechanism do not change so much as the blending ratio increases under lean conditions; while for stoichiometric and rich conditions, this increasing trend with blending ratio can be reproduced; but as blending ratio increases, laminar flame speed gradually changes from being overestimated to underestimated, and the best performance occurs at blending ratio equals to 0.5. For

pure AtJ-SPK, this reduced mechanism obviously underestimates the laminar flame speed. Therefore it is recommended to use the reduced mechanism obtained in Section 3.1 for pure AtJ-SPK. As pressure increases, laminar flame speed decreases. The reduced mechanism can also capture this trend under various pressures but the deviations under lean condition still remain as shown in Fig. 12(c).

3.2.4 Spatial profiles

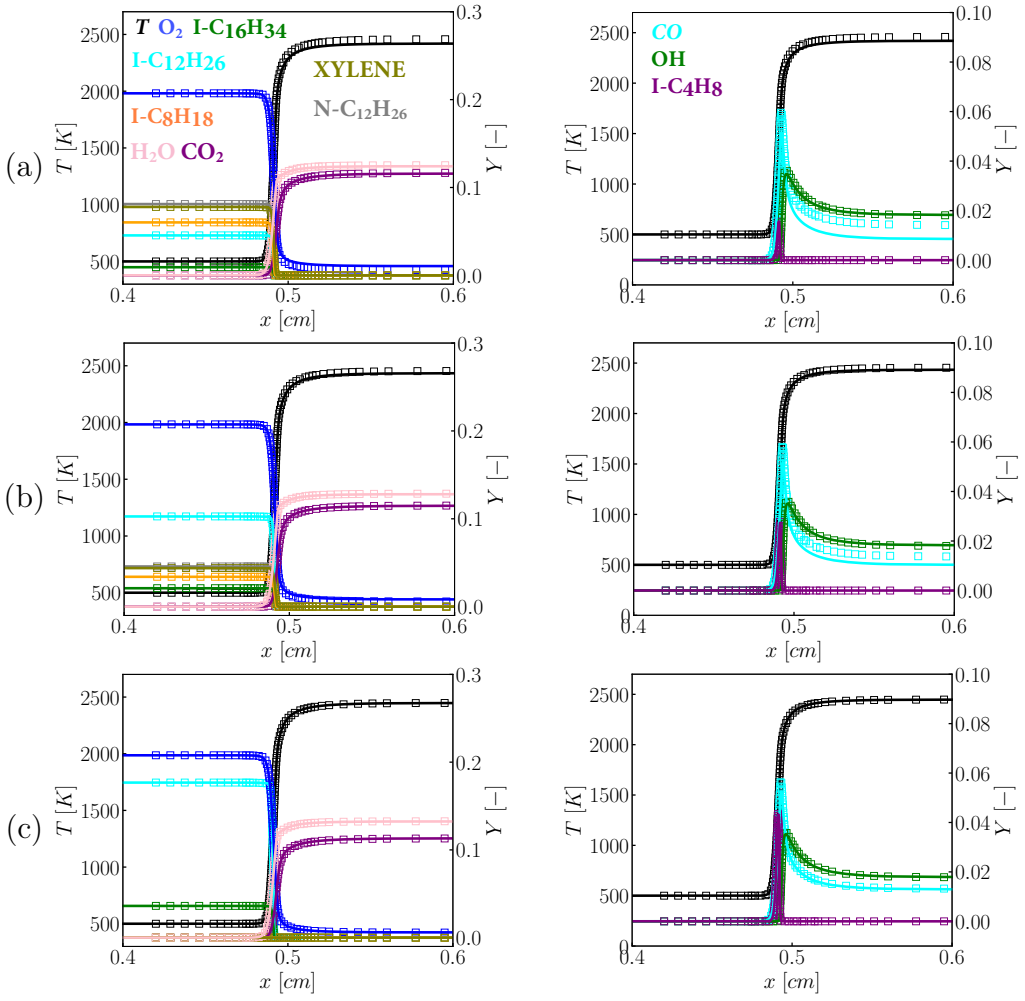

Figure 13: Comparisons of flame structures predicted using the reduced and POLIMI mechanisms under different blending ratios (ϕ = 1.0, p = 10 bar, and T_{ub} = 500 K): (a) BR = 0.2; (b) BR = 0.5; (c) BR = 1.0. Note that the profiles of major and minor species are shown in the left and right plots, respectively. OH and I-C_4H_8 mass fractions are timed with 5 and 10 for a clearer observation, respectively. Legends (species and temperature) of all the sub-figures are same and represented with colored variables in the first two plots.

The flame structures of one-dimensional (1D) freely-propagating premixed flames under various conditions are also investigated. Figure 13 shows comparisons under different blending ratios (ϕ = 1.0, p = 10 bar, and T_{ub} = 500 K). Note that only the regions of interest (reaction zones) are shown here for brevity. The flame structures predicted using the reduced mechanism are in very good agreements with those of the POLIMI mechanism. In particular, the predicted profiles of temperature, AtJ-SPK and Jet A fuel components, and products (H_2O and CO_2) profiles almost coincide with the POLIMI mechanism predictions. For the minor species, OH profiles also agree well with the POLIMI mechanism predictions. However, the CO mass fractions are slightly underestimated near the burnt side at low blending ratios, which is consistent with the results in the 0D calculations as shown in Fig. 10, and this deviation gradually decreases as blending ratio increases. When the fuel is pure AtJ-SPK, the CO mass fraction profiles can be accurately reproduced.

Figure 14 demonstrates the spatial profiles of temperature and minor/major species (mass fraction) predicted using the reduced and POLIMI mechanisms under different pressures (ϕ = 1.0, BR = 0.5, and T_{ub} = 500 K). The figure legend is the same as that of Figure 13. It is noted that as pressure increases, the flame thickness becomes much thinner. Therefore, the interested regions become narrower. Generally, the flame structure under different pressures can be accurately reproduced by the reduced mechanism. In particular, temperature and fuel/products species profiles predicted using the developed reduced mechanism agree very well with the POLIMI mechanism predictions. Note that with the increasing of pressure, the CO and OH mass fractions decrease and CO_2 mass fraction increases on the burnt side, which can be reproduced by the reduced mechanism. For the exact values, OH profiles can also be accurately reproduced. However, CO mass fractions are slightly underestimated near the burnt side, and pressure does not have a significant effect on this underestimation.

Figure 15 demonstrates comparisons in reproducing the flame structure under different equivalence ratios (p = 1 bar, BR = 0.5, and T_{ub} = 500 K). The reduced mechanism performs well in predicting the temperature and major species (fuel species and products) profiles at

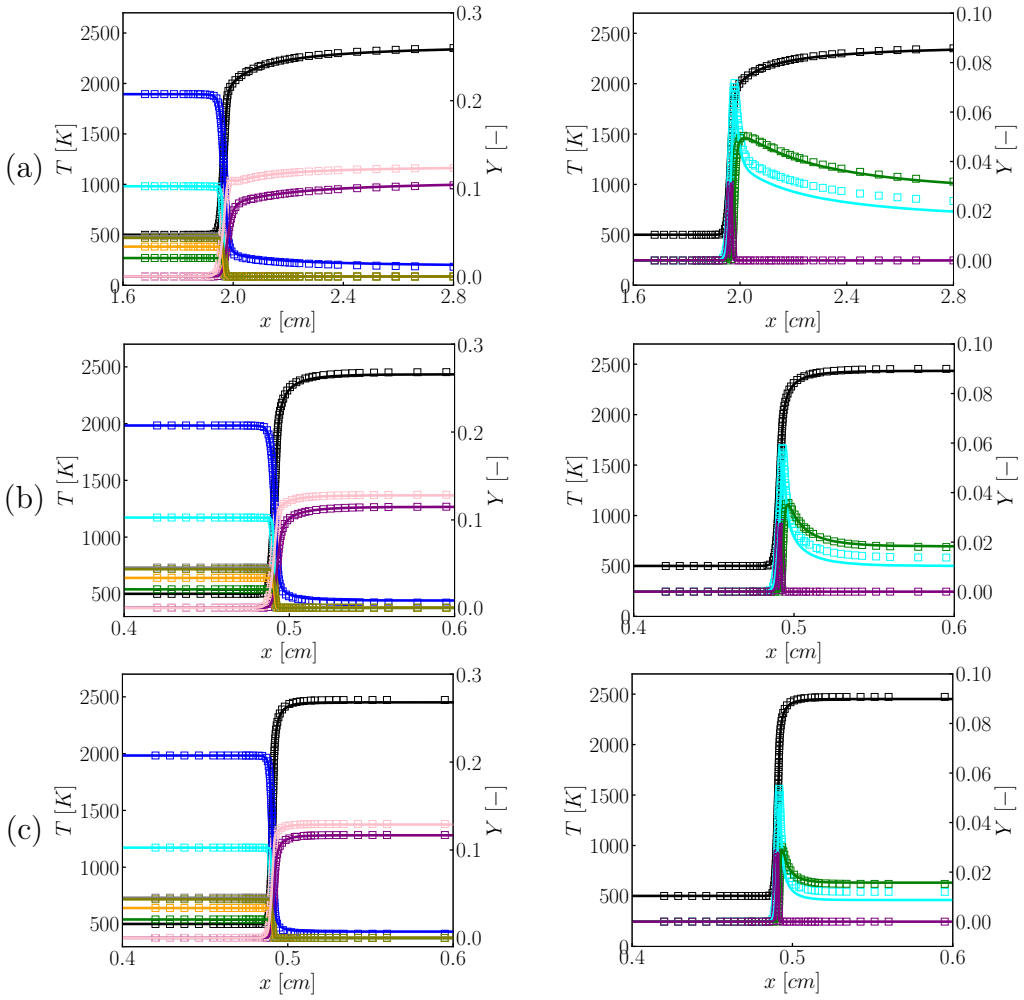

Figure 14: Comparisons of flame structures predicted using the reduced and POLIMI mechanisms under different pressures (ϕ = 1.0, BR = 0.5, and T_{ub} = 500 K): (a) p = 1 bar; (b) p = 10 bar; (c) p = 20 bar. The legend is same as that of Figure 13.

both lean-/stoichiometric-/rich- conditions. For the minor species, the reduced mechanism can give accurate predictions on OH for both the three equivalence ratios. However, under the rich condition (ϕ=1.6), the CO mass fraction is slightly underestimated in the near-burnt and burnt regions, and the relative error is less than 5%. The reduced mechanism can also well reproduce the flame structures under different temperatures at the fresh side, as shown in Fig. 16. Similar as those in other conditions, the temperature and major species (fuel species and products) profiles can be accurately predicted. The underestimation of CO mass fraction in the burnt side still remains at both the three unburnt temperatures, and the unburnt temperature does not affect this underestimation.

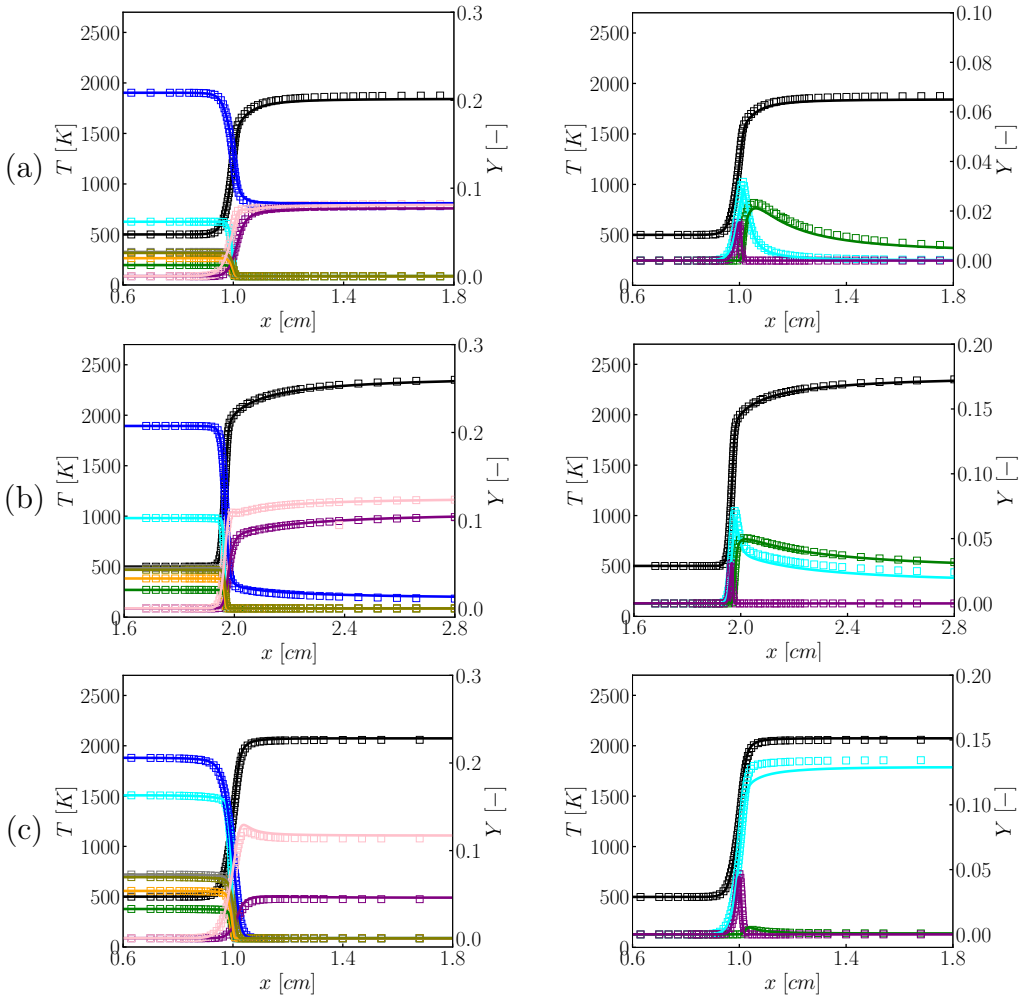

Figure 15: Comparisons of flame structures predicted using the reduced and POLIMI mechanisms under different equivalence ratios (p = 1 bar, BR = 0.5, and T_{ub} = 500 K): (a) ϕ = 0.6; (b) ϕ = 1.0; (c) ϕ = 1.6. The legend is same as that of Figure 13.

In summary, the reduced mechanism can accurately reproduce the flame structure (profiles of fuel species, OH, and products) predicted using the POLIMI mechanism under various conditions. However, CO mass fraction is slightly underestimated in the near-burnt and burnt regions, and the relative error is less than 5%. Note that for pure AtJ-SPK, it is recommended to use the reduced mechanism developed from the LLNL-AtJ-SPK in Section 3.1 as much better predictions on ignition delay times and laminar flame speeds can be obtained for pure AtJ-SPK, through comparing with the experimental data[4] (see the Supporting Information).

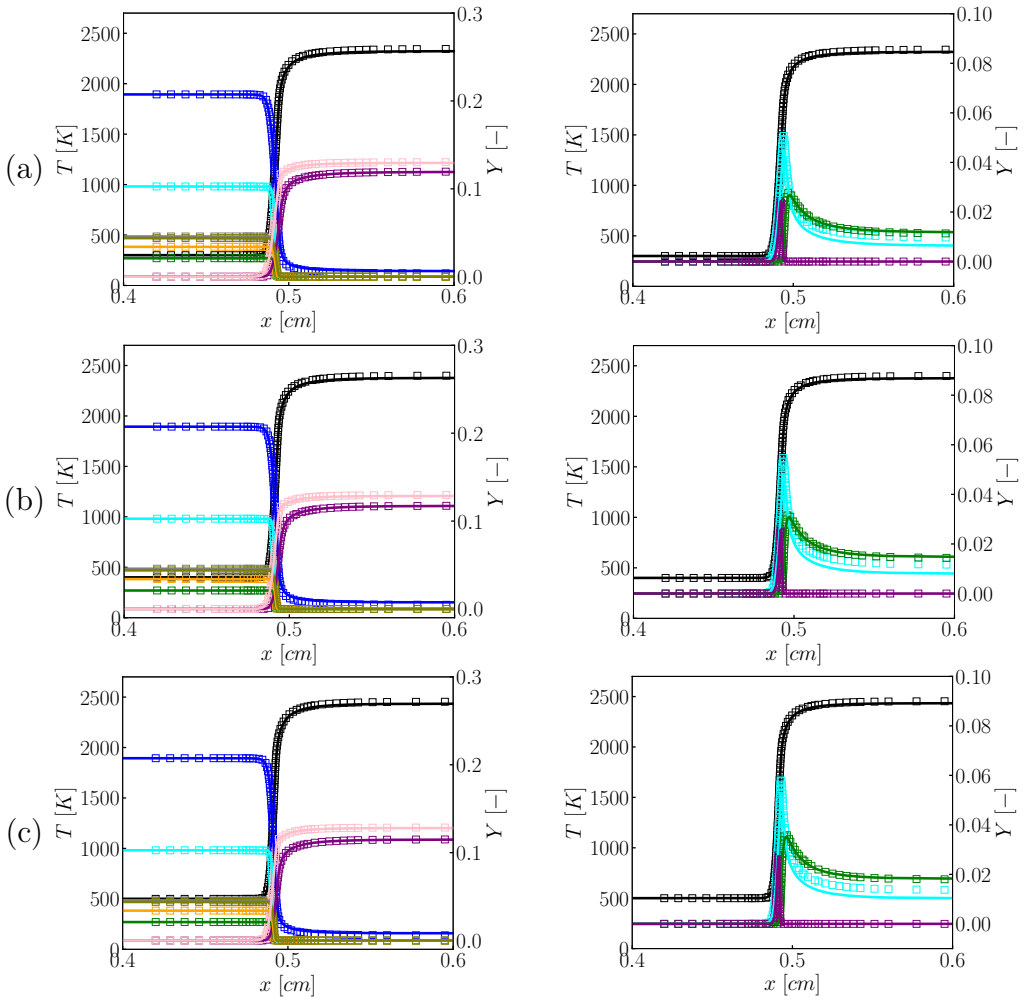

Figure 16: Comparisons of flame structures predicted using the reduced and POLIMI mechanisms under different unburnt temperatures (p = 10 bar, BR = 0.5, and phi = 1.0): (a) T_{ub} = 300 K; (b) T_{ub} = 400 K; (c) T_{ub} = 500 K. The legend is same as that of Figure 13.

4 Computational cost analysis

As demonstrated above, the developed reduced mechanisms can accurately reproduce predictions of the master detailed mechanisms on ignition delay time, laminar flame speed, and temporal/spatial profiles of gas temperature and major/minor species. The computational cost is also an important concern in numerical simulations. In this part, the computational costs of reduced and master detailed mechanisms are compared and discussed under different dimensions of calculation.

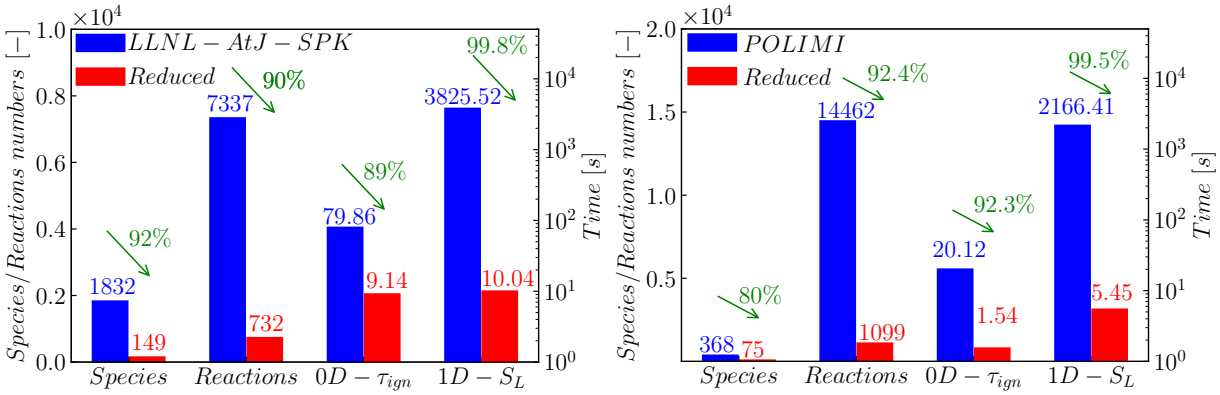

Figure 17: Comparisons of the mechanism size and computational cost of the reduced and master detailed mechanisms (Left: reduced/detailed LLNL-AtJ-SPK mechanism; Right: reduced/detailed POLIMI mechanism).

Figure 17 shows the comparisons of mechanism size and computational cost. As for pure AtJ-SPK combustion, the corresponding reduced mechanism can reduce the numbers of species and reactions by 92% and 90%, respectively, compared with those of the LLNL-AtJ-SPK mechanism. For the 0D ignition delay calculations, the reduced mechanism can reduce the computational time by 89%. While for the laminar flame speed calculations (1D freely-propagating premixed flame), the reduction percentage could reach 99.8%. Regarding the developed reduced mechanism for AtJ-SPK/Jet A blends, the species number is reduced by 80%, from 368 to 75. This reduction percentage is slightly lower than that for pure AtJ-SPK, which is because the mean reaction number per species in the POLIMI mechanism (39.2)[22] is much higher than that in the LLNL-AtJ-SPK mechanism (4.0).[4] Therefore, it is relatively hard to deeply reduce the species number. The reaction number is reduced by 92.4%, from 14462 to 1099. For the 0D ignition delay calculations, the mean calculation time for one case is decreased by 92.3%, from 20.12 to 1.54 seconds. For calculations of the 1D freely propagating premixed flames, the mean computational time for one case is reduced by 99.5%, from 2166.41 to 5.45 seconds. We also test the computational cost of reduced and master detailed mechanisms on the Fugaku Supercomputer for direct numerical simulations (DNS) of spray flames of AtJ/SPK and its blends with Jet A in a two-dimensional (2D) temporally evolving jet (0.26 million grids), which has a similar configuration as that in our

previous study.[55] Note that because the static memory needs to be attributed to all species scalars in the DNS and the maximum memory for one computational node in FUGAKU is fixed and relatively limited, 32 cores and 8 cores are used in each computational node (48 cores) when using the reduced and master detailed mechanisms, respectively. As for the developed reduced mechanism for pure AtJ-SPK, 192 seconds are required for one time-step calculation using 8 nodes, 256 cores. However, when the LLNL-AtJ-SPK detailed mechanism is used, one time-step cannot be successfully calculated within 24 hours (32 nodes, 256 cores). The computational cost could be reduced by more than 5000 times for the 2D calculations, which indicates the computational efficiency could be significantly improved by three orders of magnitude. As for the developed reduced mechanism for AtJ-SPK/Jet A blends, 239.83 seconds are required for the calculation of 0.1 ms physical time. However, it takes 31736.84 seconds when using the POLIMI detailed mechanism. The computational cost of the present developed reduced mechanism only account for 1.89% of that of the POLIMI detailed mechanism in the 2D DNS calculation, which means calculation speed could be impressively accelerated by more than 529 times.

5 Conclusions

In the present study, reduced mechanisms were developed for pure AtJ-SPK and its blends with Jet A from the LLNL-AtJ-SPK and POLIMI detailed mechanisms, respectively. The DRGEP, DRGPFA, and FSSA methods were used sequentially during the reduction process. The developed reduced mechanisms can achieve 80%/92.4% and 92%/90% reductions of the species/reaction numbers for pure AtJ-SPK and its blends with Jet A, respectively, compared with those of the master detailed mechanisms. The developed reduced mechanisms were comprehensively proven to well reproduce the ignition delay times, laminar flame speeds, and temporal/spatial profiles predicted using the master detailed mechanisms and measured in the experiments under various conditions. The computational cost comparison demonstrated

that the developed reduced mechanisms can impressively accelerate the calculation speed by more than 5000 and 529 times for 2D-DNSs of spray flames of pure AtJ-SPK and its blends with Jet A, respectively.

Supporting Information

The supporting information contains the following three materials and their descriptions are also listed below.

- SI.pdf: Comparisons of laminar flame speeds and ignition delay times predicted by the POLIMI detailed mechanism and measured in the experiments; Comparisons of performances of the reduced LLNL-AtJ-SPK and POLIMI mechanisms for pure AtJ-SPK combustion.

- Reduced-LLNL-AtK-SPK.zip: This material provides the CHEMKIN, Cantera and OpenFOAM formats of the reduced LLNL-AtK-SPK mechanism for the convenience of potential users.

- Reduced-POLIMI.zip: This material provides the CHEMKIN, Cantera and OpenFOAM formats of the reduced POLIMI mechanism for the convenience of potential users.

Note that since the OpenFOAM thermo-physical module does not support PLOG reactions, the users need to artificially alter the reaction kinetic parameters under their operation pressures, and the operation pressure is 1 bar in the provided OpenFOAM formats of the reduced mechanisms.

Acknowledgment

The authors thank the support from Japan Society for the Promotion of Science (Grant No: 21P20351). This work used computational resources of the supercomputer Fugaku provided by RIKEN through the HPCI System Research Project (Project ID: hp220141).

References

(1) Emissions, E. G. G.; Change, C. Overview of Greenhouse Gases. *Available at:[Google Scholar]* **2017**,

(2) ATAG (Aviation Transport Action Group), Aviation: Benefits Beyond Borders, Full Report. https://aviationbenefits.org/downloads/aviation-benefits-beyond-borders-2020/, 2020; [Online; last accessed 11 December 2022].

(3) Kousoulidou, M.; Lonza, L. Biofuels in aviation: Fuel demand and CO2 emissions evolution in Europe toward 2030. *Transportation Research Part D: Transport and Environment* **2016**, *46*, 166–181.

(4) Richter, S.; Kukkadapu, G.; Westbrook, C. K.; Braun-Unkhoff, M.; Naumann, C.; Köhler, M.; Riedel, U. A combined experimental and modeling study of combustion properties of an isoparaffinic alcohol-to-jet fuel. *Combustion and Flame* **2022**, *240*, 111994.

(5) Holladay, J.; Abdullah, Z.; Heyne, J. Sustainable aviation fuel: Review of technical pathways. **2020**,

(6) ASTM D4054, Standard Practice for Evaluation of New Aviation Turbine Fuels and Fuel Additives. https://www.astm.org/Standards/D7566.htm, 2023; [Online; last accessed 30 June 2023].

(7) ASTM D7566, Standard Specification for Aviation Turbine Fuel Containing Synthesized Hydrocarbons. https://www.astm.org/Standards/D7566.htm, 2022; [Online; last accessed 11 December 2022].

(8) Won, S. H.; Veloo, P. S.; Dooley, S.; Santner, J.; Haas, F. M.; Ju, Y.; Dryer, F. L. Predicting the global combustion behaviors of petroleum-derived and alternative jet fuels by simple fuel property measurements. *Fuel* **2016**, *168*, 34–46.

(9) Flora, G.; Balagurunathan, J.; Saxena, S.; Cain, J. P.; Kahandawala, M. S.; DeWitt, M. J.; Sidhu, S. S.; Corporan, E. Chemical ignition delay of candidate drop-in replacement jet fuels under fuel-lean conditions: A shock tube study. *Fuel* **2017**, *209*, 457–472.

(10) Valco, D. J.; Min, K.; Oldani, A.; Edwards, T.; Lee, T. Low temperature autoignition of conventional jet fuels and surrogate jet fuels with targeted properties in a rapid compression machine. *Proceedings of the Combustion Institute* **2017**, *36*, 3687–3694.

(11) Wang, K.; Xu, R.; Parise, T.; Shao, J.; Movaghar, A.; Lee, D. J.; Park, J.-W.; Gao, Y.; Lu, T.; Egolfopoulos, F. N., et al. A physics-based approach to modeling real-fuel combustion chemistry–IV. HyChem modeling of combustion kinetics of a bio-derived jet fuel and its blends with a conventional Jet A. *Combustion and Flame* **2018**, *198*, 477–489.

(12) Park, J.-W.; Xu, R.; Lu, T.; Wang, H. Skeletal and reduced model of NOx formation in C1 (GEVO ATJ) synthetic jet fuel. https://web.stanford.edu/group/haiwanglab/HyChem/pages/download.html, 2019; [Online; last accessed 11 December 2022].

(13) Wang, H.; You, X.; Joshi, A. V.; Davis, S. G.; Laskin, A.; Egolfopoulos, F.; Law, C. K. USC Mech Version II. High-temperature combustion reaction model of H2/CO/C1-C4 compounds. *URL: http://ignis. usc. edu/USC_ Mech_ II. htm* **2007**,

(14) Zhang, Y.; Dong, W.; Smith, G.; Wang, H. Uncertainty minimization for an alcohol-to-jet (ATJ) combustion reaction model. *13th U. S. National Combustion Meeting* **2022**,

(15) Guzman, J.; Kukkadapu, G.; Brezinsky, K.; Westbrook, C. Experimental and modeling study of the pyrolysis and oxidation of an iso-paraffinic alcohol-to-jet fuel. *Combustion and Flame* **2019**, *201*, 57–64.

(16) Vasu, S. S.; Davidson, D. F.; Hanson, R. K. Jet fuel ignition delay times: Shock tube experiments over wide conditions and surrogate model predictions. *Combustion and flame* **2008**, *152*, 125–143.

(17) Malewicki, T.; Gudiyella, S.; Brezinsky, K. Experimental and modeling study on the oxidation of Jet A and the n-dodecane/iso-octane/n-propylbenzene/1, 3, 5-trimethylbenzene surrogate fuel. *Combustion and Flame* **2013**, *160*, 17–30.

(18) Xu, R.; Wang, K.; Banerjee, S.; Shao, J.; Parise, T.; Zhu, Y.; Wang, S.; Movaghar, A.; Lee, D. J.; Zhao, R., et al. A physics-based approach to modeling real-fuel combustion chemistry–II. Reaction kinetic models of jet and rocket fuels. *Combustion and Flame* **2018**, *193*, 520–537.

(19) Munzar, J.; Akih-Kumgeh, B.; Denman, B.; Zia, A.; Bergthorson, J. An experimental and reduced modeling study of the laminar flame speed of jet fuel surrogate components. *Fuel* **2013**, *113*, 586–597.

(20) Hui, X.; Kumar, K.; Sung, C.-J.; Edwards, T.; Gardner, D. Experimental studies on the combustion characteristics of alternative jet fuels. *Fuel* **2012**, *98*, 176–182.

(21) Dooley, S.; Won, S. H.; Chaos, M.; Heyne, J.; Ju, Y.; Dryer, F. L.; Kumar, K.; Sung, C.-J.; Wang, H.; Oehlschlaeger, M. A., et al. A jet fuel surrogate formulated by real fuel properties. *Combustion and flame* **2010**, *157*, 2333–2339.

(22) Ranzi, E.; Frassoldati, A.; Grana, R.; Cuoci, A.; Faravelli, T.; Kelley, A. P.; Law, C. K. Hierarchical and comparative kinetic modeling of laminar flame speeds of hydrocarbon and oxygenated fuels. *Progress in Energy and Combustion Science* **2012**, *38*, 468–501.

(23) Lawrence Livermore National Laboratory, LLNL Mechanism. https://combustion.llnl.gov/mechanisms, 2023; [Online; last accessed 4th January 2023].

(24) Wang, H.; Dames, E.; Sirjean, B.; Sheen, D.; Tangko, R.; Violi, A.; Lai, J.; Egolfopoulos, F.; Davidson, D.; Hanson, R., et al. A high-temperature chemical kinetic model of n-alkane (up to n-dodecane), cyclohexane, and methyl-, ethyl-, n-propyl and n-butyl-cyclohexane oxidation at high temperatures. *JetSurF version* **2010**, *2*, 19.

(25) Narayanaswamy, K.; Pitsch, H.; Pepiot, P. A component library framework for deriving kinetic mechanisms for multi-component fuel surrogates: Application for jet fuel surrogates. *Combustion and Flame* **2016**, *165*, 288–309.

(26) Dagaut, P.; Cathonnet, M. The ignition, oxidation, and combustion of kerosene: A review of experimental and kinetic modeling. *Progress in energy and combustion science* **2006**, *32*, 48–92.

(27) Strelkova, M.; Kirillov, I.; Potapkin, B.; Safonov, A.; Sukhanov, L.; Umanskiy, S. Y.; Deminsky, M.; Dean, A.; Varatharajan, B.; Tentner, A. Detailed and reduced mechanisms of jet a combustion at high temperatures. *Combustion science and technology* **2008**, *180*, 1788–1802.

(28) Shastry, V.; Riber, E.; Gicquel, L.; Cuenot, B.; Bodoc, V. Large Eddy Simulations of complex multicomponent swirling spray flames in a realistic gas turbine combustor. *Proceedings of the Combustion Institute* **2023**, *39*, 2693–2702.

(29) Wang, K.; Xu, R.; Parise, T.; Shao, J.; Movaghar, A.; Lee, D. J.; Park, J.-W.; Gao, Y.; Lu, T.; Egolfopoulos, F. N., et al. A physics-based approach to modeling real-fuel

combustion chemistry–IV. HyChem modeling of combustion kinetics of a bio-derived jet fuel and its blends with a conventional Jet A. *Combustion and Flame* **2018**, *198*, 477–489.

(30) Park, J.-W.; Xu, R.; Lu, T.; Wang, H. Skeletal and reduced model of NOx formation in C1/A2 jet fuel blend. https://web.stanford.edu/group/haiwanglab/HyChem/pages/download.html, 2019; [Online; last accessed 11 December 2022].

(31) Kitano, T.; Nishio, J.; Kurose, R.; Komori, S. Evaporation and combustion of multicomponent fuel droplets. *Fuel* **2014**, *136*, 219–225.

(32) Stagni, A.; Esclapez, L.; Govindaraju, P.; Cuoci, A.; Faravelli, T.; Ihme, M. The role of preferential evaporation on the ignition of multicomponent fuels in a homogeneous spray/air mixture. *Proceedings of the Combustion Institute* **2017**, *36*, 2483–2491.

(33) Bonanni, M.; Ihme, M. Interaction of preferential evaporation and low-temperature chemistry in multicomponent counterflow spray flames. *Proceedings of the Combustion Institute* **2022**,

(34) Wang, H. Personal communication, May 16th, 2023.

(35) Pepiot-Desjardins, P.; Pitsch, H. An efficient error-propagation-based reduction method for large chemical kinetic mechanisms. *Combustion and Flame* **2008**, *154*, 67–81.

(36) Sun, W.; Chen, Z.; Gou, X.; Ju, Y. A path flux analysis method for the reduction of detailed chemical kinetic mechanisms. *Combustion and Flame* **2010**, *157*, 1298–1307.

(37) Rabitz, H.; Kramer, M.; Dacol, D. Sensitivity analysis in chemical kinetics. *Annual review of physical chemistry* **1983**, *34*, 419–461.

(38) Dooley, S.; Won, S. H.; Heyne, J.; Farouk, T. I.; Ju, Y.; Dryer, F. L.; Kumar, K.; Hui, X.; Sung, C.-J.; Wang, H., et al. The experimental evaluation of a methodology

for surrogate fuel formulation to emulate gas phase combustion kinetic phenomena. *Combustion and Flame* **2012**, *159*, 1444–1466.

(39) Felden, A.; Esclapez, L.; Riber, E.; Cuenot, B.; Wang, H. Including real fuel chemistry in LES of turbulent spray combustion. *Combustion and Flame* **2018**, *193*, 397–416.

(40) Lu, T.; Law, C. K. A directed relation graph method for mechanism reduction. *Proceedings of the Combustion Institute* **2005**, *30*, 1333–1341.

(41) Sharma, D.; Mahapatra, S.; Garnayak, S.; Arghode, V. K.; Bandopadhyay, A.; Dash, S.; Reddy, V. M. Development of the Reduced Chemical Kinetic Mechanism for Combustion of H2/CO/C1–C4 Hydrocarbons. *Energy & Fuels* **2020**, *35*, 718–742.

(42) Hockett, A.; Hampson, G.; Marchese, A. J. Development and validation of a reduced chemical kinetic mechanism for computational fluid dynamics simulations of natural gas/diesel dual-fuel engines. *Energy & Fuels* **2016**, *30*, 2414–2427.

(43) Niemeyer, K. E.; Sung, C.-J.; Raju, M. P. Skeletal mechanism generation for surrogate fuels using directed relation graph with error propagation and sensitivity analysis. *Combustion and flame* **2010**, *157*, 1760–1770.

(44) Saraee, H. S.; Hughes, K. J.; Shi, S.; Ingham, D. B.; Pourkashanian, M. Skeletal and Compact Validated Mechanisms for Iso-dodecane Using a Decoupling Methodology. *Energy & Fuels* **2023**, *37*, 2307–2318.

(45) Zhang, L.; Qi, Q. A reduced mechanism for the combustion of gasoline-ethanol blend on advanced engine combustion modes. *Fuel* **2021**, *300*, 120951.

(46) CHEMKIN-PRO, Release, 15112, Reaction Design. *Inc., San Diego, CA* **2011**, *422*.

(47) Jiang, X.; Deng, F.; Yang, F.; Huang, Z. Ignition delay characteristics and kinetic investigation of dimethyl ether/n-pentane binary mixtures: interpreting the effect of

the equivalence ratio and dimethyl ether blending. *Energy & Fuels* **2018**, *32*, 3814–3823.

(48) Harman-Thomas, J. M.; Kashif, T. A.; Hughes, K. J.; Pourkashanian, M.; Farooq, A. Experimental and modelling study of hydrogen ignition in CO2 bath gas. *Fuel* **2023**, *334*, 126664.

(49) Pichler, C.; Nilsson, E. J. Reduced kinetic mechanism for methanol combustion in spark-ignition engines. *Energy & Fuels* **2018**, *32*, 12805–12813.

(50) Zhichao, W.; Yuzhen, L.; Jianchen, W.; Zhang, C.; Zhijun, P. Experimental study on NOx emission correlation of fuel staged combustion in a LPP combustor at high pressure based on NO-chemiluminescence. *Chinese Journal of Aeronautics* **2020**, *33*, 550–560.

(51) Xiao, H.; Luo, K.; Jin, T.; Xing, J.; Chai, M.; Fan, J. The effects of swirling partially premixed flame on scaled kinetic energy transport in a gas turbine-like combustor. *Proceedings of the Combustion Institute* **2022**,

(52) Van Oijen, J.; Donini, A.; Bastiaans, R.; ten Thije Boonkkamp, J.; De Goey, L. State-of-the-art in premixed combustion modeling using flamelet generated manifolds. *Progress in Energy and Combustion Science* **2016**, *57*, 30–74.

(53) Honzawa, T.; Kai, R.; Hori, K.; Seino, M.; Nishiie, T.; Kurose, R. Experimental and numerical study of water sprayed turbulent combustion: Proposal of a neural network modeling for five-dimensional flamelet approach. *Energy and AI* **2021**, *5*, 100076.

(54) Pillai, A. L.; Inoue, S.; Shoji, T.; Tachibana, S.; Yokomori, T.; Kurose, R. Investigation of combustion noise generated by an open lean-premixed H2/air low-swirl flame using the hybrid LES/APE-RF framework. *Combustion and Flame* **2022**, *245*, 112360.

(55) Xing, J.; Luo, K.; Wang, H.; Jin, T.; Cai, R.; Fan, J. A DNS study on temporally evolving jet flames of pulverized coal/biomass co-firing with different blending ratios. *Proceedings of the Combustion Institute* **2021**, *38*, 4005–4012.